The morphology of simulated trade-wind congestus clouds under wind shear

Kevin Christopher Helfer[1,1] and Louise Nuijens[1,1]

[1]Delft University of Technology

November 30, 2022

Abstract

A growing body of literature investigates convective organisation, but few studies to date have sought to investigate how wind shear plays a role in the spatial organization of shallow (trade-wind) convection. The present study hence investigates the morphology of precipitating marine cumulus convection using large-eddy-simulation experiments with zonal forward and backward shear and without shear. One set of simulations includes evaporation of precipitation, promoting for cold-pool development, and another set inhibits evaporation of precipitation and thus cold-pool formation. Without (or with only weak) subcloud-layer shear, conditions are unfavourable for convective deepening, as clouds remain stationary relative to their subcloud-layer roots so that precipitative downdrafts interfere with emerging updrafts. Under subcloud-layer forward shear, where the wind strengthens with height (a condition that is commonly found in the trades), clouds move at greater speed than their roots, and precipitation falls downwind away from emerging updrafts. Forward shear in the subcloud layer appears to promote the development of stronger subcloud circulations, with greater divergence in the cold-pool area downwind of the original cell and larger convergence and stronger uplift at the gust front boundary. As clouds shear forward, a larger fraction of precipitation falls outside of clouds, leading to more moistening within the cold pool (gust front).

The morphology of simulated trade-wind convection and cold pools under wind shear

K. C. Helfer[1], L. Nuijens[1]

[1]Department of Geoscience and Remote Sensing, Delft University of Technology, Delft, The Netherlands

Key Points:

- Without cold pools, new convection is triggered upwind of existing cells, and with cold pools, new convection is triggered downwind.
- In the absence of (or with only weak) subcloud-layer shear, rain falls into emerging updrafts, hindering the development of convection and cold pools.
- Uplift at the cold-pool gust fronts is strongest under subcloud-layer forward shear (increasing wind speed with height).

Corresponding author: Kevin Helfer, `k.c.helfer.tud@posteo.net`

Abstract

A growing body of literature investigates convective organisation, but few studies to date
have sought to investigate how wind shear plays a role in the spatial organization of shal-
low (trade-wind) convection. The present study hence investigates the morphology of
precipitating marine cumulus convection using large-eddy-simulation experiments with
zonal forward and backward shear and without shear. One set of simulations includes
evaporation of precipitation, promoting for cold-pool development, and another set in-
hibits evaporation of precipitation and thus cold-pool formation. Without (or with only
weak) subcloud-layer shear, conditions are unfavourable for convective deepening, as clouds
remain stationary relative to their subcloud-layer roots so that precipitative downdrafts
interfere with emerging updrafts. Under subcloud-layer forward shear, where the wind
strengthens with height (a condition that is commonly found in the trades), clouds move
at greater speed than their roots, and precipitation falls downwind away from emerg-
ing updrafts. Forward shear in the subcloud layer appears to promote the development
of stronger subcloud circulations, with greater divergence in the cold-pool area down-
wind of the original cell and larger convergence and stronger uplift at the gust front bound-
ary. As clouds shear forward, a larger fraction of precipitation falls outside of clouds, lead-
ing to more moistening within the cold pool (gust front).

Plain Language Summary

The most common type of clouds in Earth's trade wind-regions are precipitating
cumulus clouds with tops up to 4 km height. The precipitation from such clouds is fre-
quent and intense enough to cause so-called cold pools: cold dried air that spreads out
laterally near the surface in a circular fashion triggering new clouds in arc-like patterns.
We used a high-resolution atmospheric model to investigate how the morphology of such
clouds and the associated cold pools is affected by vertical changes in the wind speed (shear).
When the wind speed at the surface and at cloud base is the same, clouds remain above
their 'roots', and downward-moving air associated with rain falls into those cloud roots,
which hinders the consequent deepening of these clouds. When the wind speed increases
from the surface to cloud base (which it often does), clouds move away from their roots,
which separates the location of updrafts and downdrafts, allowing for the development
of deeper clouds. Formation of new clouds at the edge of cold pools depends on the shear

too. Even when we artificially inhibit the development of cold pools, deep clouds (with tops up to 10 km) still develop in our model simulations.

1 Introduction

Triggered by the World Climate Research Programme's grand challenge on clouds, circulation and climate sensitivity (Bony et al., 2015), tremendous research efforts have been undertaken in recent years to study maritime shallow clouds, with an increasing interest in their organisation. A culmination was the EUREC[4]A field campaign in 2020 (Stevens et al., 2021), which also motivated the successful classification of trade-wind cloud patterns by their visual appearance from space into classes called fish, flower, sugar and gravel (Stevens et al., 2019). This classification indicates that the dominant pattern of trade-wind convection is not the unorganised, non-precipitating cumulus humilis cloud (sugar) but rather the somewhat deeper, precipitating congestus (gravel) that may have a stratiform outflow (flower) at greater heights (Schulz et al., 2021, in review). This finding motivates us to shed more light specifically on cumulus congestus clouds from large-eddy simulations (LES) using a set-up that differs from the traditional BOMEX and ATEX cases that have been intensely used in the past decades (Nuijens & Siebesma, 2019).

Surface wind speed (and to lesser extent wind shear) is considered as one of the predictors of the aforementioned cloud patterns (Bony et al., 2020; Schulz et al., 2021, in review). Helfer et al. (2020) (hereafter: HNRS20) ran idealised large-eddy simulations (LES) to investigate the effect of wind shear on trade-wind cumulus convection, differentiating between backward shear (BS), where surface winds weaken with height, and forward shear (FS), where surface winds strengthen with height. Indicative of their representativeness of the trades, these simulations are dominated by clouds that resemble gravel, which sometimes have stratiform outflows near clouds tops that resemble flowers. A main result in HNRS20 is that any absolute amount of wind shear limits the strength of cloud updrafts because of a stronger downward-oriented pressure perturbation force (as found in studies of deep convection, e.g. Peters et al., 2019). As a consequence, cloud deepening is hampered in the presence of shear. However, under FS, convection appears to have a tendency to grow deeper, which seems related to this system's enhanced potential to aggregate column moisture on mesoscales. Another noteworthy observation of HNRS20 is that wind anomalies within cold pools depend on the direction of the shear. This may hint at a possible role of downdrafts introducing different cloud-layer momen-

tum in the surface and subcloud layers. In modelling studies of deep convective cold pools, convective momentum transport (CMT) has been found to significantly influence cold-pool winds (Mahoney et al., 2009; Grant et al., 2020). HNRS20 speculated about the role of wind shear in the triggering of new convection at cold-pool edges.

It has long been known that cold-pool edges can trigger secondary convection (e.g. Zipser, 1969; Warner et al., 1979; Intrieri et al., 1990; Weckwerth & Wakimoto, 1992) for which several (not necessarily mutually exclusive) mechanisms are being discussed in the literature. A purely thermodynamic mechanism involves enhanced moisture and thus buoyancy at the edges of cold pools, favouring convection (Tompkins, 2001; Seifert & Heus, 2013; Romps & Jeevanjee, 2016). Using a cloud-resolving model, Tompkins (2001) showed that during the development of deep convective cold pools, evaporation of precipitation cools and moistens the boundary layer. The cold pool's gust front is consequently moister than the cold-pool centre. The lowered temperature can quickly recover, which removes nearly all convective inhibition (CIN) and allows new convection to develop in response to minimal lifting. In the reduced entrainment 'near environment' hypothesis (Böing et al., 2012; Schlemmer & Hohenegger, 2014), the interplay of moisture aggregation at cold-pool edges (as opposed to depletion of moisture inside cold pools) and vertical uplift at the leading edge of the cold pool's gravity current promotes the formation of wider, and thus deeper clouds less affected by entrainment. Gaining ground in recent literature is the dynamical or mechanical mechanism, whereby the leading edge of the cold pool's spreading gravity current is associated with a band of horizontal convergence in the wind field, which triggers uplift (Xue et al., 2008; Böing et al., 2012; Li et al., 2014; Torri et al., 2015; Meyer & Haerter, 2020). As moist near-surface air is lifted to higher levels above the level of free convection (LFC), it can moisten the upper boundary layer and lower troposphere, and trigger new convective events. This forced uplift may be enhanced by the collision of two or more cold-pool fronts (e.g. Feng et al., 2015; Meyer & Haerter, 2020).

In their LES study of a specific RICO day, Li et al. (2014) found little evidence that supports a thermodynamic mechanism for shallow convection. Inspired by studies on mid-latitude squall lines (Rotunno et al., 1988; Weisman & Rotunno, 2004), they pointed out a possible role of wind shear in the tilting of updrafts and clouds, which decides whether precipitation can fall into pre-existing cold pools and possibly strengthen them. In their simulations, the vorticity of the cold-pool boundary is weaker than that of the ambient

wind profile, and the updraft thus tilts away from the cold pool, gaining access to converged moisture at the cold-pool boundary, which is advantageous for convective development. Hence, it seems plausible that this process could help explain the cloud-top-height differences between FS and BS that were reported in HNRS20. A recent study by Mulholland et al. (2021) focusing on squall-line deep convection also notes that forced uplift is larger under stronger subcloud-layer shear as it helps larger mass fluxes and deeper clouds.

In our present study, we aim to address why cloud deepening may be inhibited more under BS than under FS in the presence and absence of cold pools. We describe the morphology of shallow convective systems under shear in idealised large-domain LES with and without the evaporation of precipitation. By turning off evaporation, we limit the formation of cold pools and thus the organization of convection in arc-shaped bands surrounding cold pools. We utilised a computational domain of 50×50 km^2, which is sufficiently large for cold-pool organisation (Seifert & Heus, 2013).

The remainder of this paper is structured as follows. In the following section, we shortly review the simulation set-up as well as the additional simulations we ran for the present paper. We then present the results in a twofold manner. First, we discuss the effects of wind shear on cold pools and the triggering of new convection at their fronts. Second, we ask how clouds behave under wind shear before cold pools emerge, by analysing simulations in which cold-pool formation is suppressed. Finally, we discuss and summarise our findings in a concluding section.

2 Experimental design

We utilised the same experimental set-up as in HNRS20 and only point out its most important aspects here. Using version 4.2 of the Dutch Atmospheric Large-Eddy Simulation model (DALES; Heus et al., 2010), we simulated an idealised shallow cumulus case, typical of the North Atlantic trades (Fig. 1). Our domain has a size of $50.4 \times 50.4 \times 17.9$ km^3, with a grid spacing of 100 m in the horizontal and a non-uniform vertical grid (stretched from 10 m at the surface to 190 m at the top). Simulations were run for 48 h, to allow for the development of sufficient precipitation. Advection was computed by a 5th-order scheme in the horizontal and a 2nd-order scheme in the vertical, and a Galilean transform was performed to reduce advective errors. We deployed a single-moment microphysics scheme that includes ice and allows for precipitation (Grabowski, 1998; Böing
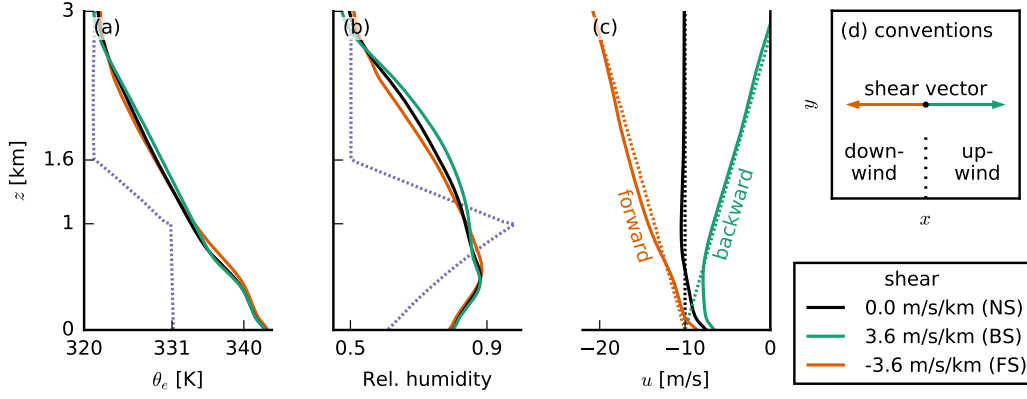
Figure 1: (a–c) Profiles of (a) equivalent potential temperature θ_e, (b) relative humidity and (c) the zonal wind components u. Dotted lines are initial profiles and solid lines indicate profiles that are averaged over the last 10 hours of the STD simulations. Orange stands for forward shear (FS), black for no shear (NS), green for backward shear (BS) and purple profiles are the same in all simulations. This colour coding is the same for all other figures. (d) Schematic of the directional conventions used in this paper: downwind is in the negative x-direction, upwind in the positive x-direction.

et al., 2012). The model uses an isotropic eddy-diffusivity approach to parametrise sub-grid turbulence.

For the sensible and latent surface heat fluxes, we prescribed $SHF = 15.3$ W m^{-2} and $LHF = 225.2$ W m^{-2}, respectively. These values allow for the development of the cloud species that we are interested in: cumulus congestus, which are somewhat deeper than shallow cumuli. The use of constant fluxes removes interactions between cold pools and surface fluxes, including those that could enhance or inhibit thermodynamic mechanisms of triggering convection. While over land interactive surface enthalpy fluxes are crucial for cold-pool modelling, Gentine et al. (2016) suggested that over oceans they only matter for cold pools of scales much larger than our domain. The surface momentum flux was computed interactively by the model, which implies that simulations that develop stronger surface winds (e.g. under FS) also develop larger surface friction. Interactions between the density current and surface friction may matter for setting the scales of cold pools and organisation (Stephan, 2021), but are not explored here. We applied a constant radiative cooling rate of -2.5 K/d to the liquid water potential temperature
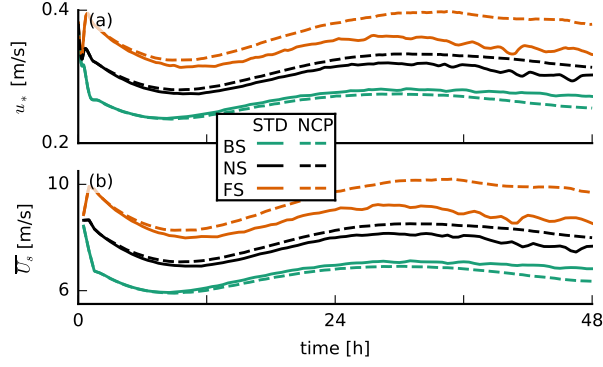
Figure 2: Time series of (a) the surface friction velocity u_* and (b) the domain-averaged total wind speed at 5 m height U_s. As explained in Fig. 1, orange indicates forward shear (FS), black no shear (NS) and green backward shear (BS), while solid lines indicate the standard (STD) runs and dashed lines the no-cold-pool (NCP) runs. The line colours and types are the same in all following figures, unless indicated otherwise.

θ_l. Large-scale subsidence was calculated interactively, using a weak-temperature-gradient approach (WTG; Daleu et al., 2012). The total water specific humidity q_t was nudged towards its initial profile above 4 km with a time scale of 6 h to avoid spurious moisture tendencies.

To investigate the dependence of shallow convection and cold pools on vertical wind shear, we ran experiments with different wind profiles (Fig. 1c). As discussed by HNRS20, backward shear, where surface easterlies weaken with height and turn westerlies eventually, is by far the most common in the North Atlantic trades. However, forward shear, where surface easterlies strengthen with height, occasionally occurs as well, in particular in July and August. The analysis of HNRS20 revealed distinct differences in the effect that shear has on convection when it is forward as opposed to backward. The authors further showed that the strength of shear does not play a major role. Hence, we here investigated three different zonal wind profiles with either no shear (NS, black line in Fig. 1c), backward shear (BS, green, $\partial_z u = 3.6 \times 10^{-3}$ s^{-1}) or forward shear (FS, orange, $\partial_z u = -3.6 \times 10^{-3}$ s^{-1}). (Note that our BS and FS cases correspond to the BS-4X and FS-4X cases of HNRS20, respectively.) These wind profiles were used as both the initial profiles and the geostrophic forcing. We did not prescribe any meridional wind ($v = 0$). In the calculation of the Coriolis acceleration, we take a latitude of 15° N.

It is important to realise that the wind profiles that develop during the course of the simulation differ from the initial profiles and the geostrophic forcing. After the initialisation of the simulation, the winds evolve to reach an equilibrium after about 24 h and stay approximately constant thereafter (Fig. 2). Figure 1 shows the profiles from the end of the simulation with solid lines and the initial profiles with dotted lines. This reveals that in the subcloud layer, forward shear occurs even in the BS case, which is also a common feature of the trades (e.g. Holland & Rasmusson, 1973). The presence of forward shear in the subcloud layer is important throughout this paper.

In addition to one set of standard runs with each of the three wind profiles (labelled STD), we performed another set of experiments in which we suppressed the formation of cold pools (labelled NCP, no cold pools). To this end, we turned off the evaporation of precipitation in the LES, which Böing et al. (2012) showed to be very effective. All precipitation in these simulations reaches the surface, and no latent cooling due to the evaporation of rain occurs, which is a crucial ingredient for the formation of cold pools (e.g. Khairoutdinov & Randall, 2006).

3 Cold pools under shear

3.1 Cold-pool structure and behaviour

All our standard simulations (STD) are characterised by the gravel type of organisation including cold pools (Fig. 3). In Fig. 3, we present top-down views of the computational domain, showcasing the different structure of cold pools in our three shear cases. In these snapshots, the mean wind ($\sim u$) blows from right to left (east to west), and hence, the left is referred to as downwind, the right as upwind (see also Fig. 1d) and north would be at the top.

Cold-pool formation starts with the precipitative downdraft (rain shaft) of a deep-enough cloud. Near the surface, the cold and dense air mass spreads out laterally as a gravity current, which is reflected by the diverging wind patterns shown in Fig. 3a–c. In those snapshots, red areas have (total) wind speeds faster than the slab average and are most prominently found at the downwind front of the cold pool, where the gust front adds up to the mean wind speed. Conversely, on the upwind side of the cold pools, the cold-pool front moves against the mean wind, leading to slower total wind speeds (shown in blue).
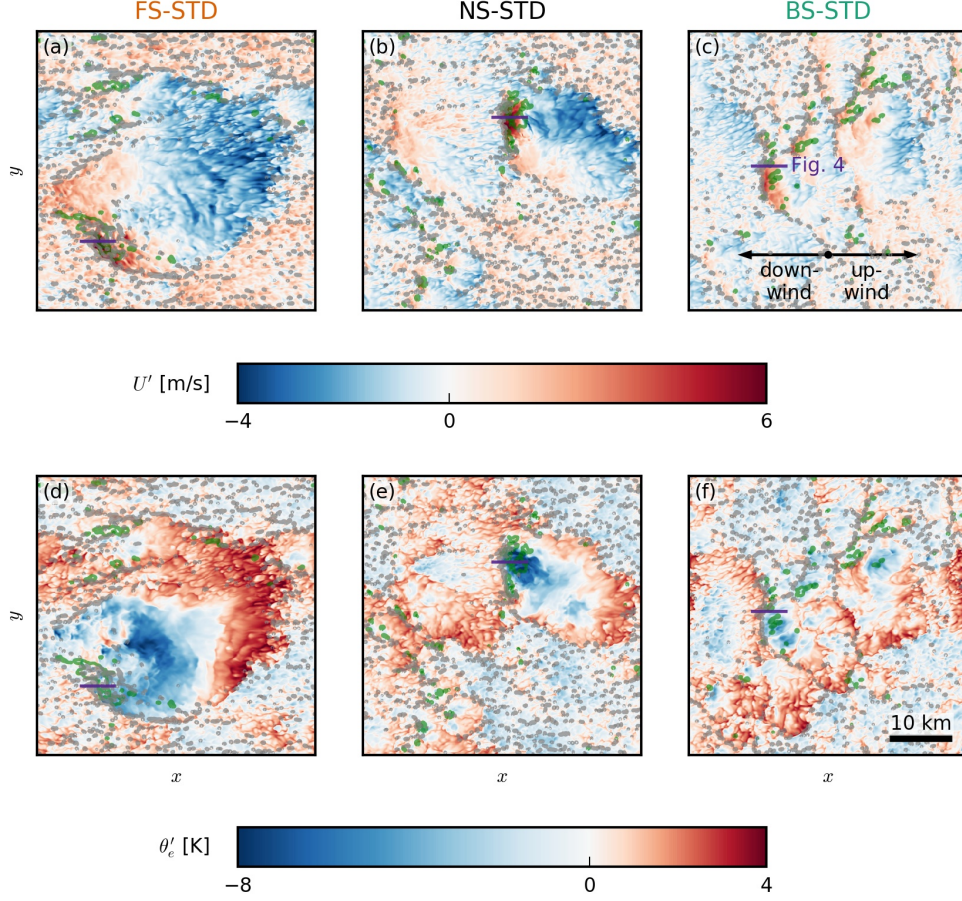
Figure 3: Snapshots of the LES domains during exemplary cold-pool events in the (a, d) FS-STD, (b, e) NS-STD and (c, f) BS-STD case. The colourmaps in the x-y cross section show (a–c) total wind speed deviations U' and (d–f) equivalent potential temperature deviations θ'_e (both from the slab average) at the lowest model level (5 m). The grey outlines indicate strong updrafts in the subcloud layer ($w = 1$ m/s at 400 m), and the green outlines indicate surface precipitation ($q_r > 0$). The snapshots were taken around 40 h. The cross sections of Fig. 4 are marked in purple.

The cold pools have a characteristic thermodynamic signature (Fig. 3d–f). Very low values of equivalent potential temperature θ_e (which combines information about the temperature and the relative humidity) are found in the centre of the cold pool, indicating that the air mass has its origin at higher altitudes where the air is cold and dry (see Fig. 1). The outermost edges of the cold pool, especially on the upwind edge, have high values of equivalent potential temperature, which indicates the presence of moist air. Because the surface fluxes are held fixed, the spatial differences in temperature and humidity may be more persistent than in nature. While in the NS and FS cases, cold pools of significant size and strength occur (like the ones in Fig. 3a and b), they are much smaller in the BS case (Fig. 3c). As we will later elaborate, they also occur more rarely in the BS and the FS cases.

Similar to what observations show, our cold pools are usually not symmetric in their appearance. Visual inspection of a large number of scenes from our simulations shows that new convection (strong subcloud-layer updrafts indicated in grey in Fig. 3) is preferably triggered at the downwind edge of the cold pools (i.e. on the left in the panels of Fig. 3), where strong winds and presumably large horizontal convergence lead to mechanical uplift (Mulholland et al., 2021).

We further investigate the vertical cloud and boundary-layer structure accompanying the exemplary cold pools from Fig. 3 by presenting vertical x-z cross section (Fig. 4). In each panel in Fig. 4, a strong precipitative downdraft is located near the right edge of the excerpt, but note that in the FS and BS cases, precipitation is or has already ceased there (see Fig. 4a, e, i). Focusing on the NS-STD case (middle row), the cold pool itself is visible as a low-temperature tongue (in terms of equivalent potential temperature θ_e) extending from the right edge of the snapshot to nearly the $x = 1$ km mark (Fig. 4f). Ahead of this cold pool (downwind), updrafts and new clouds (secondary convection) are developing near cloud base (Fig. 4e). Similar signatures of w and θ_e can be seen in the FS and BS cases. An important ingredient in the triggering of new convection by cold pools is the convergence that occurs at its downwind gust front (see Fig. 3a–c). Horizontal convergence, $C_h = -\partial_x u - \partial_y v$, between the front and the ambient wind is largest near $x = 1 \ldots 2$ km in Fig. 4c, g, k, where vertical uplift is also strong (Fig 4a, e, i). In the FS and NS cases, there is also greater zonal wind shear in the density current (upwind tilting of the cold pool boundary) as reflected by positive values of the meridional vorticity, defined as: $\omega_y = \partial_z u - \partial_x w$ (Fig 4d, h, l). In the mean or ambient wind, the
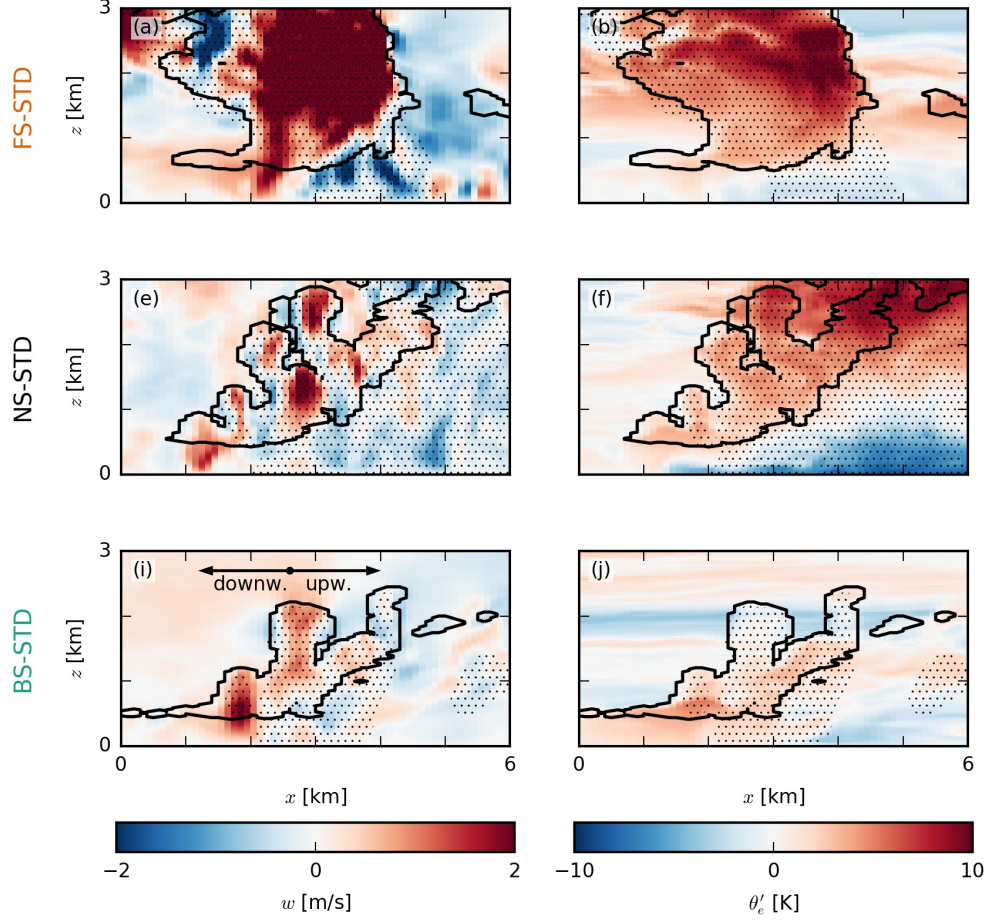
Figure 4: Snapshots of exemplary cold-pool fronts in the (a–d) FS-STD, (e–h) NS-STD and (i–l) BS-STD cases. The colourmaps in the x-z slices show (left column) the vertical velocity w and (right column) the equivalent potential temperature anomaly θ_e'. In each panel, the black outlines indicate clouds (i.e. the $q_l = 0$ isoline), the dotted areas indicate precipitation. The location of each snapshot is marked in purple in Fig. 3. Each panel is 6 km wide, averaged over 1 km in the meridional direction and taken from around 40 h (the same times as Fig. 3).
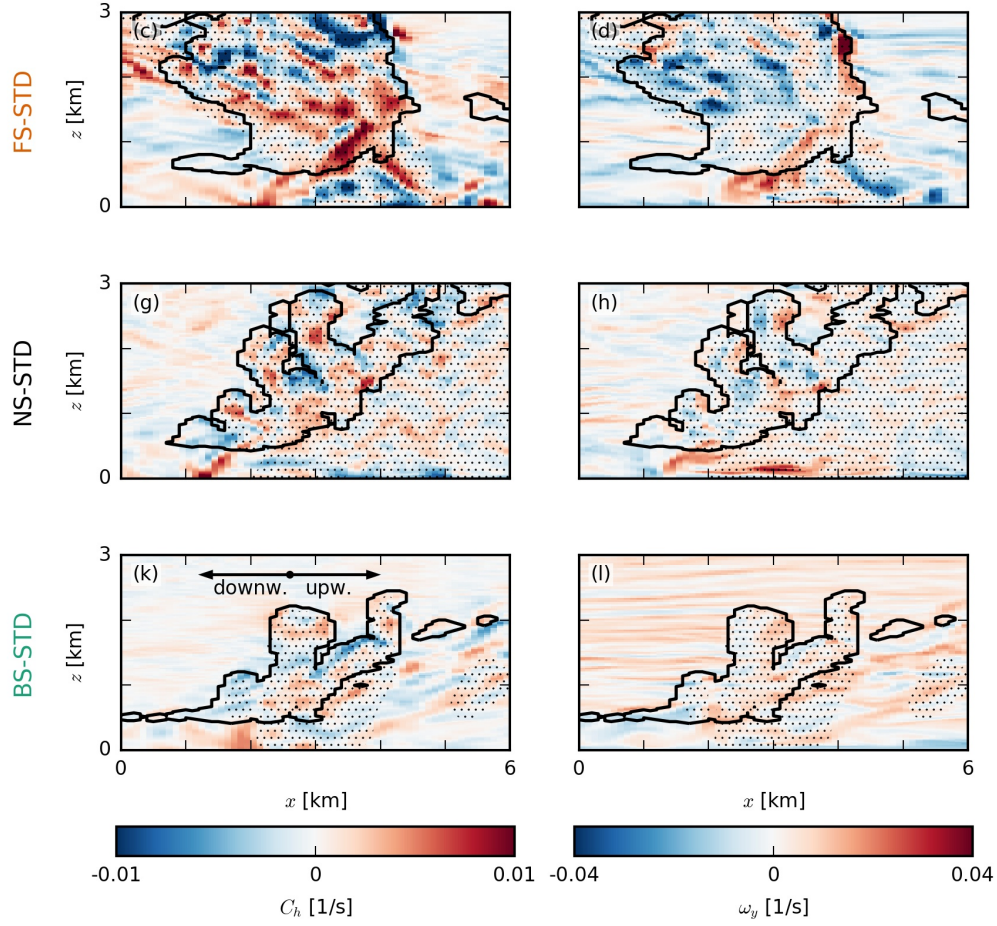
Figure 4: (continued) The colourmaps in the x-z slices show (left column) the horizontal convergence C_h and (right column) the meridional component of the vorticity ω_y.

236 subcloud-layer vorticity is instead negative (left edge of Fig. 4d, h, l), as winds tend to

237 increase with height away from the surface where they experience the strongest friction.

238 In the FS and NS cases, the density current is apparently much stronger (compared to

239 the BS case).

3.2 Convergence, vorticity and uplift at cold-pool fronts

241 The above figures are merely some exemplary snapshots, but we may analyse prob-

242 ability density functions (PDFs) of the entire domain at specific heights to support these

243 impressions (Fig. 5). In addition, we construct composite profiles conditioned on all cold-

244 pool gust fronts as well as the ambient environment (Fig. 6). To this end, we classify columns

245 as belonging to a cold pool if $\theta_e' < -2$ K at the lowest model level (where the prime

246 indicates anomalies with respect to the slab average). The equivalent potential temper-

247 ature is a commonly used quantity to identify cold pools (e.g. Zuidema et al., 2012; Schlem-

248 mer & Hohenegger, 2014). From this sample, we can identify the downwind gust front

249 through positive anomalies of the total wind speed U' (see Fig. 3a–c). We focus on the

250 period from 24 h to 36 h when convection is still shallow and cold-pool fractions are small.

251 Note that with our sampling approach it is not possible to capture profiles of convergence

252 and updrafts at the gust front because they are located outside the cold pool (see Fig. 4).

253 In the PDFs in Fig. 5, we find indications of more vigorous cold-pool gust fronts

254 in the FS and NS cases. The figure shows a similar frequency of negative anomalies of

255 θ_e in all STD cases (Fig. 5a) but more frequent large values of horizontal convergence

256 and divergence in the FS and NS cases (Fig. 5b). These can be attributed to larger wind-

257 speed anomalies (Fig. 5f). The FS and NS cases also have stronger subcloud-layer up-

258 drafts (Fig. 5c), which is in line with a more idealised study of deep convective cold pools

259 by Mulholland et al. (2021) who showed that low-level (forward) shear, which is pronounced

260 in our FS and NS cases, leads to stronger, deeper and wider squall-line updrafts as well

261 as an increased mass flux.

262 Li et al. (2014) pointed out that the vorticity contrast between the cold-pool front

263 and the ambient wind profile sets the tilt of forced updrafts and therefore the degree to

264 which they may tap into existing moist air in the cold pool front or in already moistened

265 cloud air above the mixed layer and near cloud base (see their Fig. 15). With a more pro-

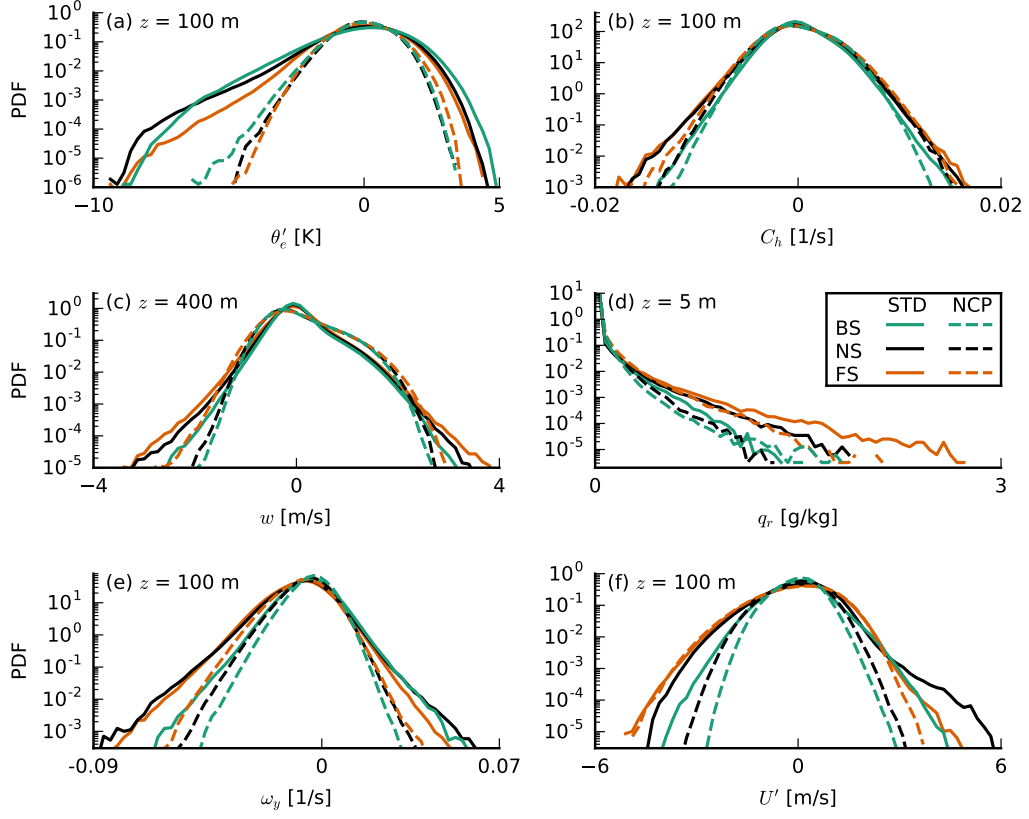266 nounced negative vorticity in the ambient wind (Fig. 5e), the updrafts are slanted for-

Figure 5: Probability density functions (PDFs) of (a) the equivalent potential temperature anomaly θ'_e at 100 m, (b) the horizontal convergence C_h at 100 m, (c) the vertical velocity w at 400 m, (d) the rain water specific humidity q_r at 5 m, (e) the meridional vorticity component ω_y at 100 m and (f) the zonal wind velocity anomaly u' at 100 m, all averaged over Hours 24–36 of each simulation. Solid lines indicate the standard simulations (STD) and dashed lines the no-cold-pools simulations (NCP).
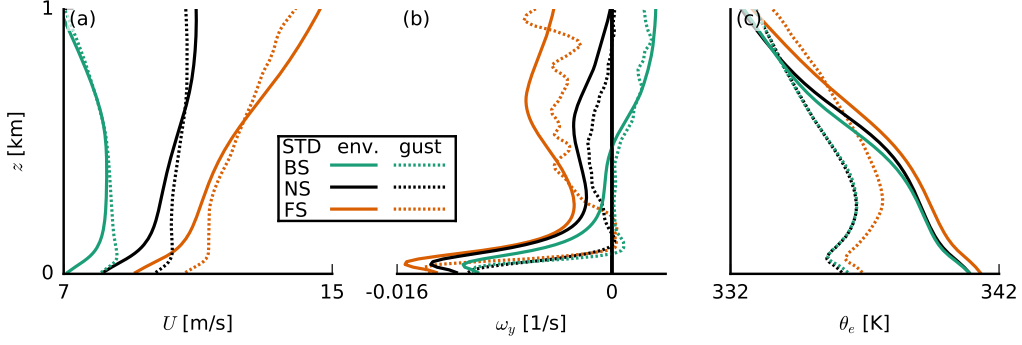
Figure 6: Composite profiles of (a) total wind speed U, (b) meridional vorticity ω_y and (c) equivalent potential temperature θ_e sampled over cold-pool gust fronts ($\theta_e' < -2$ K and $U' > 0$ at the lowest model level; dotted lines) and the environment ($\theta_e' > -2$ K), all averaged over Hours 24–36 of the STD simulations.

ward more in the FS and NS cases than in the BS case, where the gust front has zero vorticity over a much deeper layer (Fig. 6b). It is therefore unclear how a vorticity argument alone (as in the original RKW theory; Thorpe et al., 1982; Rotunno et al., 1988; Weisman & Rotunno, 2004) would lead to stronger updrafts in the FS and NS case, because slanted updrafts are generally subjected to a stronger downward-oriented pressure gradient force than updrafts that are upright. The FS case has a higher equivalent potential temperature in both the environment and the gust front (Fig. 6c), due to larger absolute humidity (not shown), which may result from more evaporated precipitation during Hours 12–24 of the simulation (see Fig. 7e), as in the FS case a larger fraction of rain falls outside of clouds (discussed in Section 4). The extra humidity would aid cloud development, but one can also imagine such differences to be quickly diminished in the presence of surface-flux feedbacks (absent in our simulations).

The largest difference in the cold-pool structure among our shear cases appears to be in the near-surface wind speed. Figure 5f shows that the FS case, followed by the NS case, has larger negative and positive wind-speed anomalies. This is not only true for the STD runs with cold pools, but also in the NCP runs where no gust fronts develop. Along with the stronger updrafts and downdrafts (Fig. 5c), this implies that the FS case has stronger circulations (see also HNRS20). CMT might play a role here. In the presence of shear, vertical (convective) transport of momentum can introduce larger wind-

286 speed anomalies. Under FS, updrafts will carry slow surface winds, introducing conver-

287 gence in a narrow updraft region through the depth of the mixed layer, while downdrafts

288 (which are displaced downwind from the updrafts under FS, as discussed below in Sec-

289 tion 4) introduce faster winds and broad regions of divergence in the raining areas. The

290 downward transport of larger momentum may be even more pronounced in the presence

291 of rain evaporation, as suggested in studies of deep convection (Mahoney et al., 2009;

292 Grant et al., 2020). CMT can help sustain or even strengthen the cold-pool circulations

293 under FS. Under BS instead, the updrafts and downdrafts are not separated in space (Sec-

294 tion 4), nor are the wind-speed anomalies introduced by transport very different.

295 Because our simulations were run with constant and homogenous surface fluxes,

296 differences in forced uplift we observe (Fig. 5c) are not caused by thermodynamic fluxes,

297 e.g. the mechanism proposed by Tompkins (2001). The only difference being wind shear,

298 it thus appears likely that the underlying cause of stronger uplift in the FS and NS cases

299 (as compared to BS) lies in the process of momentum transport.

300 As discussed in HNRS20, moisture aggregation and precipitation in our simulations

301 differ between the shear cases. In the time series in Fig. 7, we show the cold-pool frac-

302 tion, defined as the area fraction where $\theta'_e < -2$ K on the lowest model level; the av-

303 erage and maximum cloud-top height (CTH); deviations of moist static energy from the

304 domain mean within the moistest and driest quartiles (in terms of total water path) of

305 blocks of 12.6×12.6 km^2 compared to the domain mean (as a measure for moisture ag-

306 gregations; see Bretherton & Blossey, 2017); the domain-mean surface precipitation and

307 the cloud cover. Even on the first simulation day, around 16 h, the FS case begins to ag-

308 gregate moisture (Fig. 7d) and develop deeper clouds (Fig. 7b, c), which rain more (Fig. 7e)

309 and form cold pools (Fig. 7a). This advantage of the FS case underlines that subcloud-

310 layer forward shear seems to favour stronger circulations, more divergence in the cold

311 pool and more convergence and forced uplift at the outflow boundary.

312 The BS case instead seems to be at a disadvantage in the sense that it develops no

313 deep clouds and significantly less cold pools (Fig. 7a–c). In the following section we wish

314 to shed more light on this and look more closely at the triggering of convection in sim-
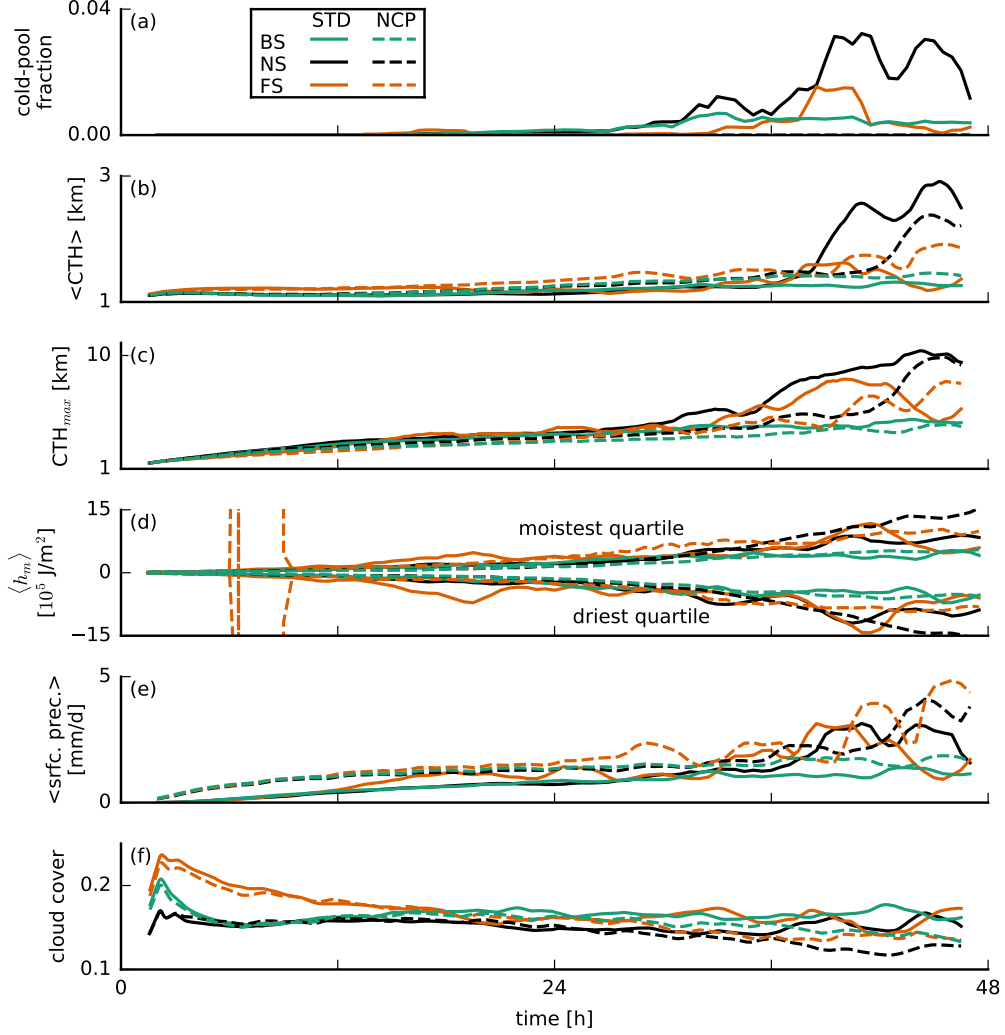
315 ulations in which cold pools are suppressed (NCP).

Figure 7: Time series of (a) the area fraction of cold pools ($\theta'_e < -2$ K) at the lowest model level, (b) average and (c) maximum cloud top height (CTH), (d) vertically integrated (up to 1 km) moist static energy anomalies $< h_m >$ in the moistest and driest quartiles of 12.6×12.6 km^2 blocks, (e) surface precipitation and (f) cloud cover. The data are smoothed using a 3-hour running-average filter.
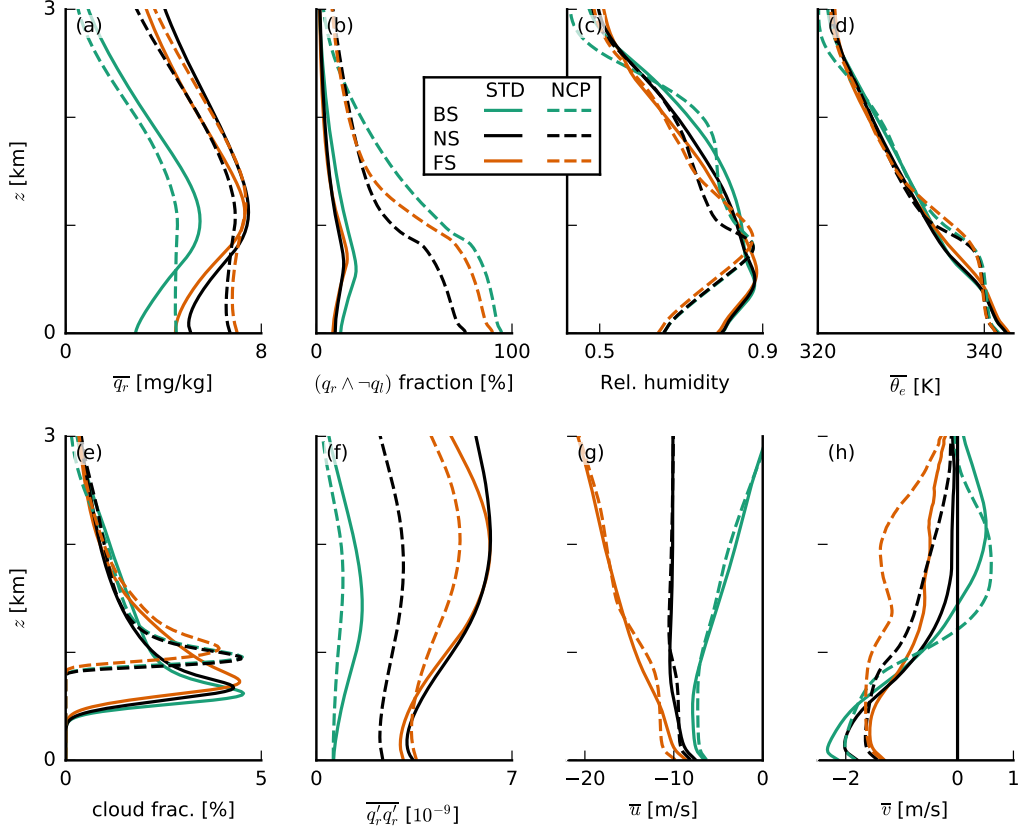
Figure 8: Slab-averaged profiles of (a) rain water specific humidity q_r, (b) the ratio of rainy grid points outside of clouds, (c) relative humidity, (d) equivalent potential temperature θ_e, (e) cloud fraction, (f) the variance of q_r, (g) zonal wind velocity u and (h) meridional wind velocity v, all averaged over the last ten hours of each simulation.

4 Sheared convection without cold pools

4.1 System development without evaporation of precipitation

Turning off the evaporation of precipitation (NCP runs) effectively suppresses cold pools (Fig. 7a), but moisture aggregation is still a common feature (Fig. 7d). Without cold pools, the thermodynamic structure of the simulated atmosphere is significantly different (Fig. 8). While the amount of rain in the cloud layer differs only little (Fig. 8a), surface precipitation is higher in the NCP runs than in the STD runs (see also Fig. 7e) because in the NCP runs all the rain reaches the surface, while in the STD runs, a large fraction evaporates in the subcloud layer (Fig. 8a). Consequently, in the NCP runs, more

grid points outside of clouds contain rain compared to the STD runs (Fig. 8b), while within clouds, the ratio is unchanged (not shown). The lack of rain evaporation in the subcloud layer leads to a decreased relative humidity there (Fig. 8c). This is caused by both the lack of transfer of rain water to water vapour and by the lack of evaporative cooling, which results in a warmer subcloud layer (Fig. 8d). Furthermore, we observe a higher cloud-base height (Fig. 8e) and a deeper mixed layer, for example evident in the temperature, relative-humidity and zonal wind profiles (Fig. 8c, d, g), which contributes to the drier boundary layer. Without evaporation of precipitation and thus cold pools, cloud tops are not significantly lower, but convective deepening is delayed by some extent (Fig. 7b–c).

4.2 Convective structure along the shear vector

Exemplary snapshots of cloud systems from the NCP simulations (Fig. 9) suggest that under FS and NS, precipitation is falling downwind from the clouds and downwind from the subcloud-layer roots of the clouds, where new updrafts develop. Under BS, precipitation tends to fall near the existing subcloud-layer updraft, which would essentially inhibit the updraft.

We may attempt to quantify where in our shear cases rain shafts are located in relation to the bulk of the clouds and liquid water. To this end, we organise the domain by column-integrated water vapour (CWV), where high CWV corresponds to regions where moisture converges to form (deep) clouds. In some sense, mapping all grid points by CWV allows us to create a cross section through the bulk water vapor and cloud structure, moving from clear sky regions (low CWV) to cloud centers (high CWV). Figure 10 shows the distribution of precipitation as a function of height and CWV. The shear cases have somewhat different distributions of CWV, but nonetheless, differences in the distribution of rain are visible. Under NS and even more under FS, the presence of rain in columns with lower CWV is evident, whereas under BS, rain water below clouds is limited to the columns with highest CWV.

The differences in the CWV-binned cloud and rain distributions do not reveal whether rain is located upwind or downwind of clouds. To quantify the precipitation's preferred direction with respect to the clouds, we perform an analysis of the cross-correlation of the cloud-water field with the rain-water field. The cross-correlation is a measure for the
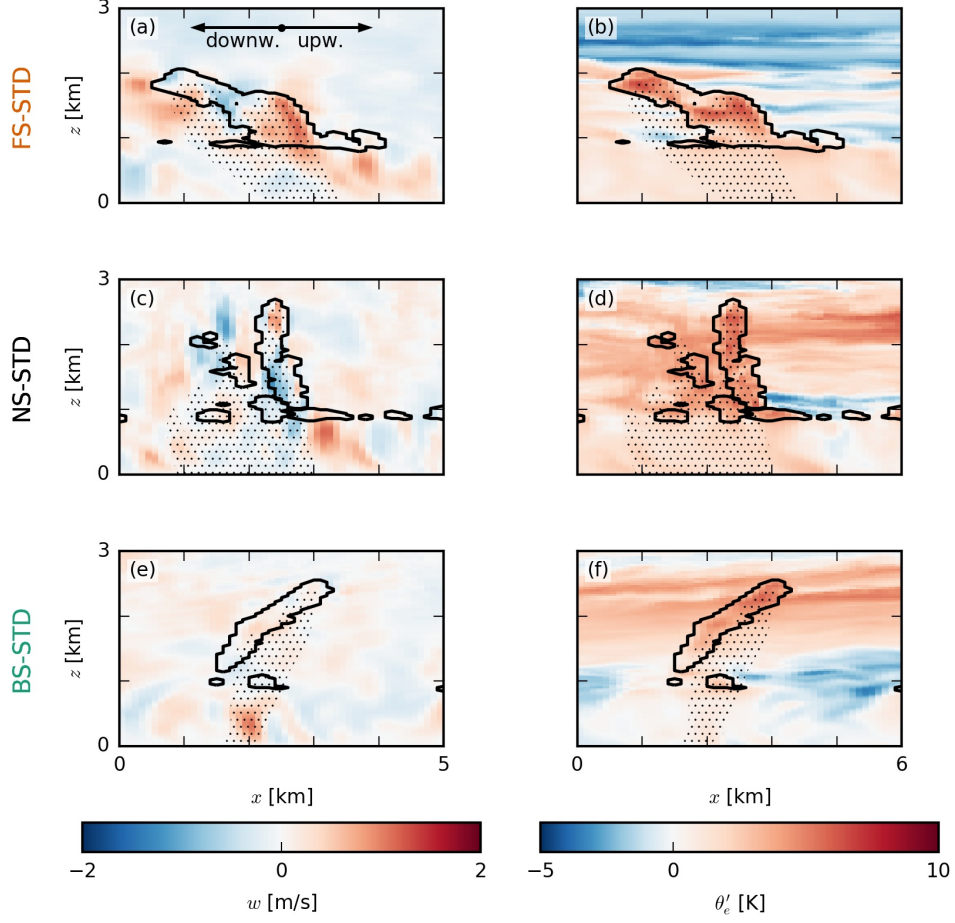
Figure 9: Snapshots of exemplary clouds in the (a–b) FS-NCP, (c–d) NS-NCP and (e–f) BS-NCP cases. The colourmaps in the x-z slices show (left column) the vertical velocity w and (right column) the equivalent potential temperature anomaly θ_e. Just as Fig. 4, the black outlines indicate clouds (i.e. the $q_l = 0$ isoline), and the dotted areas indicate precipitation. Each panel is 5 km wide, averaged over 1 km in the meridional direction and taken from the late stages of the simulation (around 40 h) to allow for a comparison with Fig. 4.
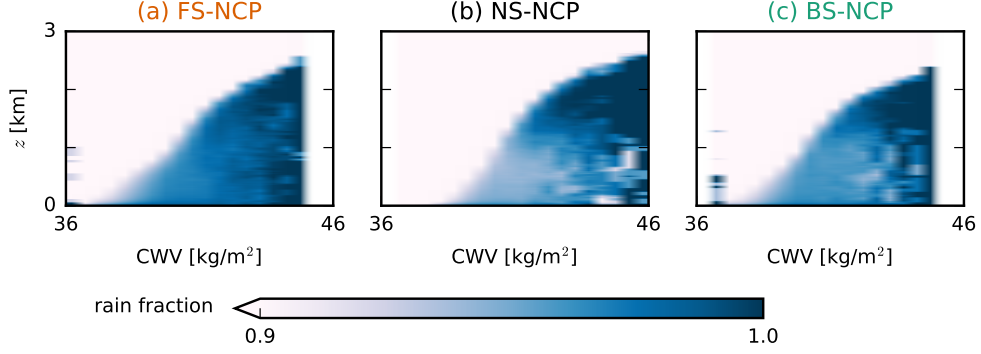
Figure 10: Composite profiles of the fraction of rainy grid points ($q_r > 0$) averaged over bins of column-integrated water vapour (CWV). All data are averaged from 30-minute output of the instantaneous 3D fields in the hours 12–18 of the NCP simulations.

similarity of two vectors as a function of shift relative to each other, which is commonly used in signal processing. Occasionally, it is also used in atmospheric science, for example to study coherent structures in the boundary layer (Schmidt & Schumann, 1989; Lohou et al., 2000). Generally, the cross-correlation of two discrete real functions f and g of length N is defined by:

$$X(\Delta) = \sum_{j=0}^{N} f(j)g(j+\Delta),\tag{1}$$

where Δ indicates the displacement (lag) of g with respect to f. We compute the cross-correlation of every row i of the q_l field (at 1 km, i.e. near cloud base) with every other row of the q_r field (averaged over the subcloud layer up to 1 km) and sum up the resulting vectors. Making use of the periodicity of the fields (i.e. $N+i \, \widehat{=} \, i$), this yields a matrix,

$$X(\Delta_i, \Delta_j) = \sum_{i=0}^{N_i} \sum_{j=0}^{N_j} q_l(i,j)q_r(i+\Delta_i, j+\Delta_j),\tag{2}$$

with positive values where similarities between the two fields occur. The 'coordinates' (Δ_i, Δ_j) of the centre of mass of this matrix are assumed to form a good measure of the offset of the precipitation field with respect to the cloud field. The time series of these coordinates in Fig. 11 shows a clear signal in the first 24 h of the simulations, especially in the x-coordinate. During this time, there is a negative x-offset of the q_r field with respect to the q_l field in the FS and NS cases of up to 100 m (Fig. 11a). A negative offset here means downwind. In the BS case, however, the x-offset is much weaker and of inconsistent sign. Thus, in the FS and NS cases, rain falls downwind of clouds, while in
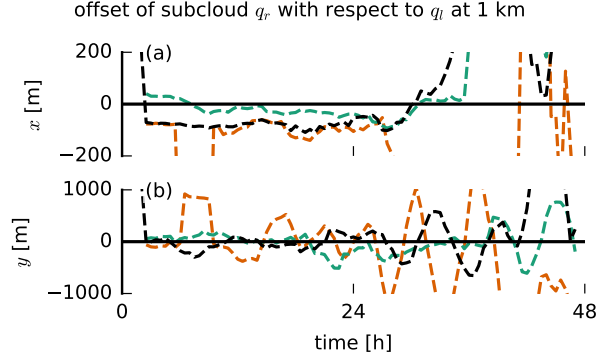
offset of subcloud q_r with respect to q_l at 1 km

Figure 11: Lateral offset in (a) x and (b) y of the rain water specific humidity field averaged over 0–1 km with respect to the liquid water specific humidity field at 1 km. The offset is computed from the centre of mass of the matrix that contains the sum of the cross-correlation vectors of each row of the q_l field with every other row of the q_r field (Eq. 2). The analysis is done on 30-minute output of the instantaneous 3D fields. For clarity, we only show the NCP simulations here.

374 the BS case, precipitation is located under clouds. Shear tilts clouds (resulting in a higher

375 projected cloud cover, see Fig. 7f), which causes part of the rain to fall out of the sides

376 of the clouds: downwind under FS and upwind under BS (as visible in Fig. 9). On the

377 second day, the convection becomes more clustered and less random and the offset sig-

378 nal thus more inconsistent. The y-offset is more incoherent (Fig. 11b), suggesting a more

379 random distribution of rain in the meridional direction, but this is not surprising given

380 that the mean wind is in the zonal direction.

381   The tendency of new updrafts to emerge upwind of existing clouds in the FS and

382 NS cases and then tilt forward (see Fig. 9) is because the subcloud layer is characterised

383 by zonal forward shear (Fig. 8g). This means that clouds move faster than their roots

384 (subcloud-layer thermals), which literally stay behind and can continue to feed moisture

385 into the cloud layer right behind (upwind) of earlier cells. In the BS case, there is only

386 little shear in the subcloud layer, and the wind speed is similar near the ground and at

387 cloud base. This implies that the roots of thermals move at the same speed as the clouds

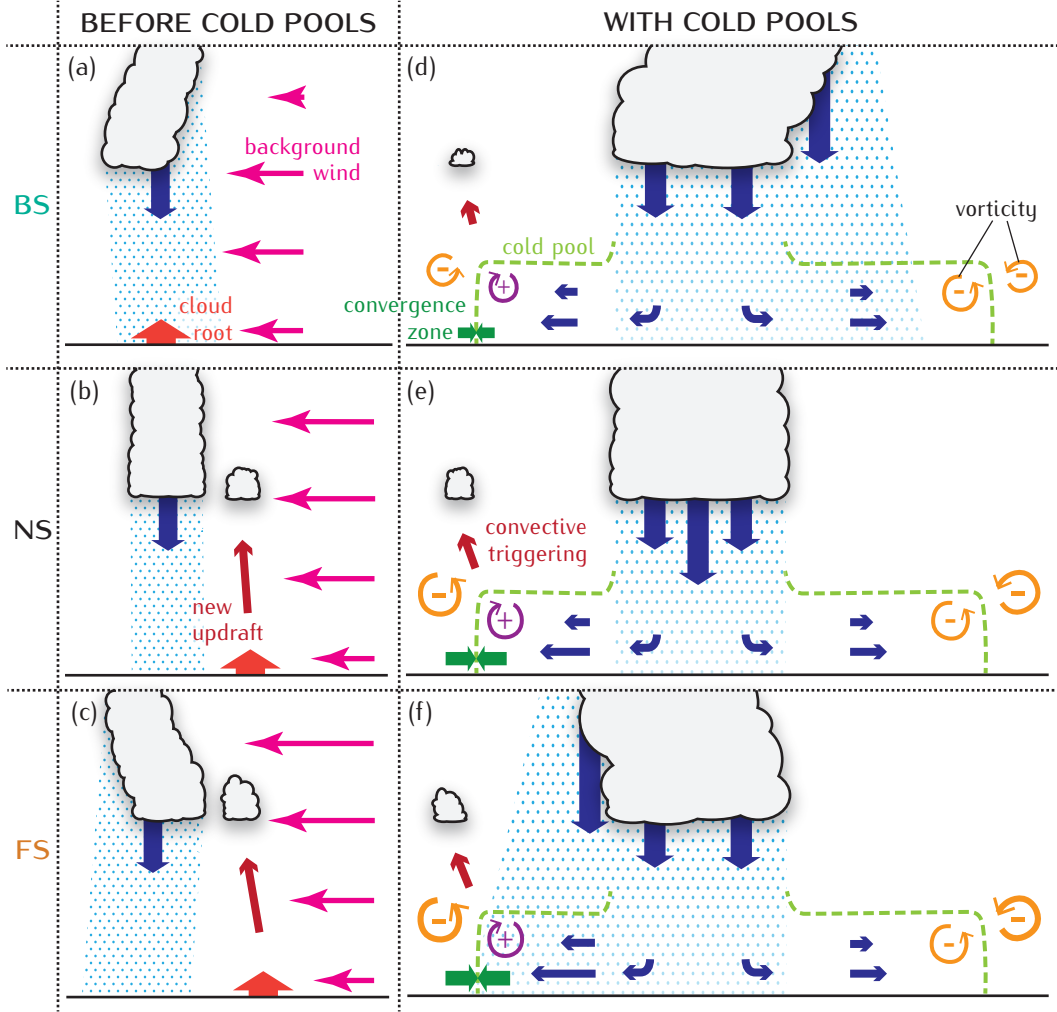388 above, making them more vulnerable to precipitative downdrafts, inhibiting the updraft.

Figure 12: Conceptual picture of (a–b) the morphology of unorganised clouds and (c–d) the structure of cold pools in (a, c) the BS case, on the one hand, and (b, d) the FS and NS cases, on the other hand.

5 Discussion and conclusion

In this paper, we used idealised LES experiments with and without cold pools and with different amounts of vertical wind shear, to investigate differences in cloud morphology and the structure of cold pools that develop due to wind shear and that may influence convective development and deepening. We find that shear has an influence on subcloud-layer circulations by separating updrafts from downdrafts, by setting the area and location of rain and rain evaporation, and thus the moistening of the subcloud layer, and by introducing different wind-speed anomalies through CMT, which may strengthen cir-

culations (divergence and convergence) and convective triggering. We summarise our findings in the schematic in Fig. 12:

1. In the BS case, precipitative downdrafts are located near or upwind of existing clouds, which is also where new updrafts are located before cold pools are present (Fig. 12a). The precipitation hence hampers new and existing convective cells in their development. In the FS and NS cases, precipitative downdrafts are located downwind, separated from the existing root and new updrafts (Fig. 12b, c).

2. Once cold pools are present, new convection is typically triggered downwind at the gust-front outflow boundary, where convergence triggers forced uplift (Fig. 12d–f). There is stronger horizontal convergence at the downwind gust front in the FS and NS cases. This facilitates the formation of stronger updrafts in these cases compared to the BS case.

3. In the FS and NS cases, the subcloud-layer is characterised by pronounced forward shear, which implies the presence of negative vorticity, which leads the updrafts to tilt more forward, possibly tapping into moister air ahead of the cold pool (Fig. 12e, f).

4. Stronger wind-speed anomalies develop under FS and NS compared to BS, even before cold pools develop and in the complete absence of cold pools. This suggests that CMT facilitates the development of stronger subcloud-layer circulations by introducing stronger winds and thus stronger divergence in the (raining) downdraft area downwind of existing cells, while introducing relatively weaker winds and thus more convergence in the updraft regions.

The mechanisms in the FS and NS cases are overall similar, as indicated in Fig. 12, because both cases have subcloud-layer forward shear. However, there are still some differences between them. For example, the FS case has a tendency to develop more column-moisture aggregations and deeper clouds at an earlier point in the simulation because this case has larger wind-speed anomalies and stronger updrafts, indicative of stronger circulations. Furthermore, the FS case has a moister subcloud layer, because of more rain evaporation. Preliminary analysis of simulations run on an even larger domain (150×150 km^2) support our findings here. On this large domain, the FS case develops deep convection with tops > 10 km and a large number of cold pools within half a day, while the BS clouds only reach 10 km after more than 40 h.

After a longer simulation time, the FS case looses its advantage over the NS case, as cold-pool fractions and cloud-top heights are lower. As shown in HSRN2020, this can be attributed to weaker cloud updrafts under FS (and BS) as compared to NS, due to a slanting of the updraft and a stronger downward oriented pressure gradient force. Additionally, precipitative downdrafts get weaker under FS, because they are subjected to more evaporation as they spread out over a larger area due to shear (Fig. 12f). Cold pools in the NS case become more vigorous in this stage because precipitation remains concentrated in narrow rain shafts. This is reflected by the significant increase of the variance of q_r (while q_r itself only increases slightly) from the NS-NCP to the NS-STD case (Fig. 8a, f), i.e. when convection transforms from more random organisation with precipitation throughout the domain (low variance) to cold pools with narrow strong rain shafts and dry areas surrounding them (high variance). On the other hand, cold pools in the FS case are less vigorous because precipitation is spread out over larger areas, as reflected in the similar variance of q_r in the FS-STD and FS-NCP cases (Fig. 8f). Furthermore, rain falling at the same downwind location where cold pools trigger new convection (see Fig. 4a) inhibits the FS case. The disadvantage of the BS case is diminished by the relocation of convective triggering to locations upwind instead of downwind once strong precipitative downdrafts lead to the formation of cold pools.

Overall, the cloud morphology is thus most favourable for convective deepening if forward shear is present in the subcloud layer (FS and NS cases) but no forward shear in the cloud layer (NS and BS cases). In the BS case, the low amount of shear in the subcloud layer and the presence of shear in the cloud layer is disadvantageous for cloud deepening, while in the FS case, only the cloud-layer shear forms a disadvantage. The NS case can ultimately develop the deepest clouds and most cold pools because it combines all advantages: forward shear in the subcloud layer and a lack of shear in the cloud layer.

HNRS20 showed that simulations with interactive surface fluxes have a similar response to wind shear as those with constant surface fluxes, and preliminary analysis suggests that this is also the case for the cold-pool characteristics presented here. Furthermore, Gentine et al. (2016) suggest that interactive surface fluxes are only of importance for cold pools over land and much larger cold pools, but further work on this question is ongoing (e.g. in the framework of EUREC[4]A; Stevens et al., 2021). It should be noted that a potential thermodynamic mechanism of triggering secondary convection (Tompkins, 2001) inherently requires interactive surface fluxes and was thus not investigated here.

Exactly because such thermodynamic feedbacks are absent and the only difference is in wind shear, our study provides evidence that the proposed mechanisms of triggering secondary convection through moisture convergence at cold-pool edges (e.g. Böing et al., 2012; Schlemmer & Hohenegger, 2014; Mulholland et al., 2021) and through mechanical uplift (e.g. Li et al., 2014; Meyer & Haerter, 2020) may be facilitated through CMT, which is known to matter for deep convective organization. This underlines the notion that it is not a single mechanism that is responsible for the triggering of secondary convection at cold-pool gust fronts (Torri et al., 2015).

Acknowledgments

References

Böing, S. J., Jonker, H. J. J., Siebesma, A. P., & Grabowski, W. W.   (2012).   Influence of the Subcloud Layer on the Development of a Deep Convective Ensemble.   *Journal of the Atmospheric Sciences*, *69*(9), 2682–2698.   doi: 10.1175/JAS-D-11-0317.1

Bony, S., Schulz, H., Vial, J., & Stevens, B.   (2020).   Sugar, Gravel, Fish, and Flowers: Dependence of Mesoscale Patterns of Trade-Wind Clouds on Environmental Conditions.   *Geophysical Research Letters*, *47*(7), 1–9.   doi: 10.1029/2019GL085988

Bony, S., Stevens, B., Frierson, D. M. W., Jakob, C., Kageyama, M., Pincus, R., ... Webb, M. J.   (2015).   Clouds, circulation and climate sensitivity.   *Nature Geoscience*, *8*(4), 261–268. doi: 10.1038/ngeo2398

Bretherton, C. S., & Blossey, P. N.   (2017).   Understanding Mesoscale Ag-

gregation of Shallow Cumulus Convection Using Large-Eddy Simulation. *Journal of Advances in Modeling Earth Systems*, *9*(8), 2798–2821. doi: 10.1002/2017MS000981

Daleu, C. L., Woolnough, S. J., & Plant, R. S. (2012). Cloud-Resolving Model Simulations with One- and Two-Way Couplings via the Weak Temperature Gradient Approximation. *Journal of the Atmospheric Sciences*, *69*(12), 3683–3699. doi: 10.1175/JAS-D-12-058.1

Feng, Z., Hagos, S., Rowe, A. K., Burleyson, C. D., Martini, M. N., & Szoeke, S. P. (2015). Mechanisms of convective cloud organization by cold pools over tropical warm ocean during the ¡scp¿AMIE/DYNAMO¡/scp¿ field campaign. *Journal of Advances in Modeling Earth Systems*, *7*(2), 357–381. doi: 10.1002/2014MS000384

Gentine, P., Garelli, A., Park, S. B., Nie, J., Torri, G., & Kuang, Z. (2016). Role of surface heat fluxes underneath cold pools. *Geophysical Research Letters*, *43*(2), 874–883. doi: 10.1002/2015GL067262

Grabowski, W. W. (1998). Toward Cloud Resolving Modeling of Large-Scale Tropical Circulations: A Simple Cloud Microphysics Parameterization. *Journal of the Atmospheric Sciences*, *55*(21), 3283–3298. doi: 10.1175/1520-0469(1998)055⟨3283:TCRMOL⟩2.0.CO;2

Grant, L. D., Moncrieff, M. W., Lane, T. P., & Heever, S. C. (2020). Shear-Parallel Tropical Convective Systems: Importance of Cold Pools and Wind Shear. *Geophysical Research Letters*, *47*(12), 1–10. doi: 10.1029/2020GL087720

Helfer, K. C., Nuijens, L., de Roode, S. R., & Siebesma, A. P. (2020). How Wind Shear Affects Trade-wind Cumulus Convection. *Journal of Advances in Modeling Earth Systems*, *12*(12). doi: 10.1029/2020MS002183

Heus, T., van Heerwaarden, C. C., Jonker, H. J. J., Siebesma, A. P., Axelsen, S., van den Dries, K., ... Vilà-Guerau de Arellano, J. (2010). Formulation of the Dutch Atmospheric Large-Eddy Simulation (DALES) and overview of its applications. *Geoscientific Model Development*, *3*(2), 415–444. doi: 10.5194/gmd-3-415-2010

Holland, J. Z., & Rasmusson, E. M. (1973). Measurements of the Atmospheric Mass, Energy, and Momentum Budgets Over a 500-Kilometer Square of Tropical Ocean. *Monthly Weather Review*, *101*(1), 44–55. doi:

10.1175/1520-0493(1973)101⟨0044:MOTAME⟩2.3.CO;2

Intrieri, J. M., Bedard, A. J., & Hardesty, R. M.   (1990).   Details of Colliding Thunderstorm Outflows as Observed by Doppler Lidar.   *Journal of the Atmospheric Sciences*, *47*(9), 1081–1099. doi: 10.1175/1520-0469(1990)047⟨1081:DOCTOA⟩ 2.0.CO;2

Khairoutdinov, M., & Randall, D.   (2006).   High-resolution simulation of shallow-to-deep convection transition over land.   *Journal of the Atmospheric Sciences*, *63*(12), 3421–3436. doi: 10.1175/JAS3810.1

Li, Z., Zuidema, P., & Zhu, P.   (2014).   Simulated convective invigoration processes at trade wind cumulus cold pool boundaries.   *Journal of the Atmospheric Sciences*, *71*(8), 2823–2841. doi: 10.1175/JAS-D-13-0184.1

Lohou, F., Druilhet, A., Campistron, B., Redelspergers, J. L., & Saïd, F.   (2000).   Numerical study of the impact of coherent structures on vertical transfers in the atmospheric boundary layer. *Boundary-Layer Meteorology*, *97*(3), 361–383. doi: 10.1023/A:1002641728075

Mahoney, K. M., Lackmann, G. M., & Parker, M. D.   (2009).   The Role of Momentum Transport in the Motion of a Quasi-Idealized Mesoscale Convective System.   *Monthly Weather Review*, *137*(10), 3316–3338.   doi: 10.1175/2009MWR2895.1

Meyer, B., & Haerter, J. O.   (2020).   Mechanical Forcing of Convection by Cold Pools: Collisions and Energy Scaling.   *Journal of Advances in Modeling Earth Systems*, *12*(11). doi: 10.1029/2020MS002281

Mulholland, J. P., Peters, J. M., & Morrison, H.   (2021).   How does vertical wind shear influence entrainment in squall lines?   *Journal of the Atmospheric Sciences*, *78*(6), 1931–1946. doi: 10.1175/jas-d-20-0299.1

Nuijens, L., & Siebesma, A. P. (2019). Boundary Layer Clouds and Convection over Subtropical Oceans in our Current and in a Warmer Climate. *Current Climate Change Reports*, *5*(2), 80–94. doi: 10.1007/s40641-019-00126-x

Peters, J. M., Hannah, W., & Morrison, H.   (2019).   The Influence of Vertical Wind Shear on Moist Thermals.   *Journal of the Atmospheric Sciences*, *76*(6), 1645–1659. doi: 10.1175/JAS-D-18-0296.1

Romps, D. M., & Jeevanjee, N.   (2016).   On the sizes and lifetimes of cold pools.   *Quarterly Journal of the Royal Meteorological Society*, *142*(696), 1517–1527.

doi: 10.1002/qj.2754

Rotunno, R., Klemp, J. B., & Weisman, M. L. (1988). A Theory for Strong, Long-Lived Squall Lines. *Journal of the Atmospheric Sciences*, *45*(3), 463–485. doi: 10.1175/1520-0469(1988)045⟨0463:ATFSLL⟩2.0.CO;2

Schlemmer, L., & Hohenegger, C. (2014). The Formation of Wider and Deeper Clouds as a Result of Cold-Pool Dynamics. *Journal of the Atmospheric Sciences*, *71*(8), 2842–2858. doi: 10.1175/JAS-D-13-0170.1

Schmidt, H., & Schumann, U. (1989). Coherent structure of the convective boundary layer derived from large-eddy simulations. *Journal of Fluid Mechanics*, *200*(D11), 511–562. doi: 10.1017/S0022112089000753

Schulz, H., Eastman, R., & Stevens, B. (2021, in review). Characterization and Evolution of Organized Shallow Convection in the Trades. *Journal of Geophysical Research*. doi: 10.1002/essoar.10505836.1

Seifert, A., & Heus, T. (2013). Large-eddy simulation of organized precipitating trade wind cumulus clouds. *Atmospheric Chemistry and Physics*, *13*(11), 5631–5645. doi: 10.5194/acp-13-5631-2013

Stephan, C. C. (2021). Mechanism for the Formation of Arc-Shaped Cloud Lines over the Tropical Oceans. *Journal of the Atmospheric Sciences*, *78*(3), 817–824. doi: 10.1175/JAS-D-20-0129.1

Stevens, B., Bony, S., Brogniez, H., Hentgen, L., Hohenegger, C., Kiemle, C., ... Zuidema, P. (2019). Sugar, gravel, fish and flowers: Mesoscale cloud patterns in the trade winds. *Quarterly Journal of the Royal Meteorological Society*, *146*(726), 141–152. doi: 10.1002/qj.3662

Stevens, B., Bony, S., Farrell, D., Ament, F., Blyth, A., Fairall, C., ... Zöger, M. (2021). EUREC⁴A. *Earth System Science Data Discussions*. doi: 10.5194/essd-2021-18

Thorpe, A. J., Miller, M. J., & Moncrieff, M. W. (1982). Two-dimensional convection in non-constant shear: A model of mid-latitude squall lines. *Quarterly Journal of the Royal Meteorological Society*, *108*(458), 739–762. doi: 10.1002/qj.49710845802

Tompkins, A. M. (2001). Organization of Tropical Convection in Low Vertical Wind Shears: The Role of Cold Pools. *Journal of the Atmospheric Sciences*, *58*(13), 1650–1672. doi: 10.1175/1520-0469(2001)058⟨1650:OOTCIL⟩2.0.CO;2

Torri, G., Kuang, Z., & Tian, Y.   (2015).   Mechanisms for convection triggering by cold pools.   *Geophysical Research Letters*, *42*(6), 1943–1950.   doi: 10.1002/2015GL063227

Warner, C., Simpson, J., Martin, D. W., Suchman, D., Mosher, F. R., & Reinking, R. F.   (1979).   Shallow Convection on Day 261 of GATE: Mesoscale Arcs.   *Monthly Weather Review*, *107*(12), 1617–1635.   doi: 10.1175/1520-0493(1979)107⟨1617:SCODOG⟩2.0.CO;2

Weckwerth, T. M., & Wakimoto, R. M.   (1992).   The Initiation and Organization of Convective Cells atop a Cold-Air Outflow Boundary. *Monthly Weather Review*, *120*(10), 2169–2187.   doi: 10.1175/1520-0493(1992)120⟨2169:TIAOOC⟩2.0.CO;2

Weisman, M. L., & Rotunno, R.   (2004).   "A Theory for Strong Long-Lived Squall Lines" Revisited. *Journal of the Atmospheric Sciences*, *61*(4), 361–382. doi: 10.1175/1520-0469(2004)061⟨0361:ATFSLS⟩2.0.CO;2

Xue, H., Feingold, G., & Stevens, B.   (2008).   Aerosol Effects on Clouds, Precipitation, and the Organization of Shallow Cumulus Convection.   *Journal of the Atmospheric Sciences*, *65*(2), 392–406. doi: 10.1175/2007JAS2428.1

Zipser, E. J.   (1969).   The Role of Organized Unsaturated Convective Downdrafts in the Structure and Rapid Decay of an Equatorial Disturbance.   *Journal of Applied Meteorology*, *8*(5), 799–814.   doi: 10.1175/1520-0450(1969)008⟨0799:TROOUC⟩2.0.CO;2

Zuidema, P., Li, Z., Hill, R. J., Bariteau, L., Rilling, B., Fairall, C., . . . Hare, J. (2012).   On trade wind cumulus cold pools.   *Journal of the Atmospheric Sciences*, *69*(1), 258–280. doi: 10.1175/JAS-D-11-0143.1